applied optics

Detection and localization of gold nanoshells inside cells: near-field approximation

Mario D'Acunto,[1,2,*] Antonio Cricenti,[2] Serena Danti,[3] Simone Dinarelli,[2] Marco Luce,[2] Davide Moroni,[1] and Ovidio Salvetti[1]

[1]Consiglio Nazionale delle Ricerche, Istituto di Scienza e Tecnologie dell'Informazione, CNR-ISTI, via Moruzzi 1, 56124 Pisa, Italy
[2]Consiglio Nazionale delle Ricerche, Istituto di Struttura della Materia, CNR-ISM, via Fosso del Cavaliere, 100, 00133 Rome, Italy
[3]Department of Surgical, Medical, Molecular Pathology and Emergency Medicine, University of Pisa, via Paradisa 2, 56124 Pisa, Italy
*Corresponding author: mario.dacunto@ism.cnr.it

Received 10 June 2016; revised 9 August 2016; accepted 9 August 2016; posted 10 August 2016 (Doc. ID 268090); published 12 September 2016

The optical properties of metal nanoparticles play a fundamental role for their use in a wide range of applications. In hyperthermia treatment, for example, gold nanoshells (NSs, dielectric core+gold shell) pre-embedded in a cancer cell absorb energy when exposed to appropriate wavelengths of a laser beam and heat up, thereby destroying the cancer cell. In this process, nevertheless, healthy tissues (not targeted by the NSs) along the laser path are not affected; this is because most biological soft tissues have a relatively low light absorption coefficient in the near-infrared (NIR) regions—a characteristic known as the tissue optical window. Over such a window, NIR light transmits through the tissues with scattering-limited attenuation and minimal heating, thereby avoiding damage to healthy tissues. As a consequence, the identification of NSs assumed a fundamental role for the further development of such cancer treatment. Recently, we have demonstrated the possibility to identify 100–150 nm diameter gold NSs inside mouse cells using a scanning near-optical microscope (SNOM). In this paper, we provide a numerical demonstration that the SNOM is able to locate NSs inside the cell with a particle–aperture distance of about 100 nm. This result was obtained by developing an analytical approach based on the calculation of the dyadic Green function in the near-field approximation. The implications of our findings will remarkably affect further investigations on the interaction between NSs and biological systems.

OCIS codes: (180.4243) Near-field microscopy; (260.3060) Infrared; (240.6680) Surface plasmons; (300.1030) Absorption.

http://dx.doi.org/10.1364/AO.55.000D11

1. INTRODUCTION

The optical properties of metallic (e.g., gold, silver) nanoparticles in the visible and near-infrared (vis–NIR) domains are based on the collective response of conduction electrons—the so-called plasmon excitations [1–4]. These form an electron gas that moves away from its equilibrium position when perturbed by an external light field, inducing surface polarization charges that act as a restoring force on the electron gas. The result is a collective oscillatory motion of the electrons characterized by a dominant resonance band that, depending by the shape and size of the metal nanoparticles, falls in the vis–NIR range [1]. Plasmons produce strong effects in both the near- and far-field response of metal nanoparticles, essentially, gold and silver. The far-field is fundamental for describing the macroscopic properties of absorption and scattering in colloidal dispersions and metamaterials. The near-field properties, instead, play a key role in describing the surroundings of the particle within a distance smaller than the wavelength of light, i.e., the optical properties between nanoparticles, the interaction with nearby molecules, and the sensing powering as in the Surface-enhanced Raman spectroscopy (SERS) techniques [5]. As an example, the near-field properties of gold NSs can act as nanolenses with near-field enhancements that vary from 3 times for gold nanoshells with outer radii of 12–15 nm and up to an enhancement factor of ∼450 for assemblies of gold nanospheres that can be thought as made of rows of nanolenses [1]. For the past two decades, the near-field has been experimentally detected via scanning near-field optical microscopy (SNOM) [6].

One biomedical application, where a combination of NSs, a NIR transparency window, and near-field optics plays a fundamental role, faces the problem of identification of NSs inside cells. The ability to identify NSs inside cells is of vital importance for medical treatments of cancers as well as for the investigation of inner cell organs and components [7–9]. Recently, we demonstrated the possibility to identify 100–150 nm diameter gold NSs inside mouse cells using an aperture SNOM [10].

In this paper, we numerically demonstrate that a SNOM with an aperture diameter of nearly 50 nm is able to locate

NSs inside the cell with a particle–aperture distance of about 100 nm. This result is obtained by developing an analytical approach based on the calculation of the dyadic Green function in the near-field approximation, and it is in good agreement with what is expected by a SNOM with a $\lambda/10$ resolution.

2. NEAR-FIELD OPTICAL PROPERTIES OF GOLD NSS AS OBSERVED BY AN APERTURE SNOM

The optical cross sections and luminescent properties of gold nanoshells compare favorably with those of conventional fluorophores or quantum dots [11–14]. The NIR power absorption of a single 20 nm diameter nanoshell can correspond to the equivalent absorption of 4×10^4 molecules of a common dye, like Indocyanine Green, used as a photosensitizer in photodynamic therapy [15]. However, the most important characteristic of gold nanoshells is their tunability. In fact, the position of the extinction peak corresponding to the plasmon resonance and the selective contributions of absorption and scattering to total extinction can be tuned by changing only two parameters: the radii of the inner core and the outer shell. This tunability is particularly important if we wish to exploit the NIR tissue window from 700 to 900 nm, where tissues are most transparent to light. The tunability in the NIR of barium titanate-gold NSs (80 nm core+ 40 nm gold shell) was recently demonstrated using Mie scattering [16,17], and the possibility to identify such NSs inside mouse cells was later evidenced experimentally using an aperture SNOM [10]. The homemade SNOM used for such study was set to operate in air in collection mode with a fixed oblique angle of illumination ($\theta = 45°$). Different illumination wavelengths ranging from visible to near-infrared were used. The homemade procedure for tip manufacturing was based on the chemical etching process, producing tips with an aperture diameter of nearly 50 nm. After the etching process, the tips were coated by a tiny metallic (evaporated aluminum) layer so as to prevent light from coupling into the fiber from anywhere other than at the aperture of the probe. In Fig. 1, we summarize the results experimentally obtained for the identification of gold nanoshells inside mouse cells, making use of an aperture SNOM [10]. In the central image of Fig. 1, the overlapping of the topography of the mouse cell and the optical map collected by the SNOM shows two dark points, which are evidenced by the arrows. Such dark points correspond to a strong

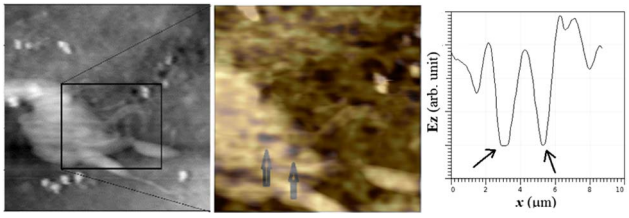

Fig. 1. (Left) 20 μm × 20 μm topography of h9c2 mouse cells recorded with a homemade aperture SNOM. (Middle) Overlapping of the topography image with the corresponding optical map. The arrows denote the NS identified within the cell. (Right) Strong-absorption points marked by arrows in the overlapping image and denoting the dimensions of the NSs. (Adapted with permission from [10].)

reduction of the collected signal by the SNOM. This is due to the high external light absorption of the NSs plasmons interacting with the external electromagnetic field.

The penetration depth of NIR light in animal cells is very high. To get an idea of how thick the cell layer must be in order to absorb the light, the extinction coefficient of the animal cell (h9c2 mouse cell in our case) is a key parameter. The penetration depth, h, as a function of wavelength can be estimated by the relation $h \approx 1/\mathrm{Im}\left[\sqrt{\epsilon_{\mathrm{cell}}(\omega)}\right]$. Being that the imaginary component of the cell dielectric function negligible, the penetration depth can reach to centimeters for a wavelength falling in the NIR range. Our single cell measurements, represented in Fig. 1, show a topography with a height of nearly 3 μm so that all the cell is practically transparent to external NIR source light.

The measurements, whose results are reported in Fig. 1, lead to a fundamental question: what is the height of the NS inside the cell? We will define this problem as the z-location question. Before detailing the analytical and numerical approaches, which are essentially based on the dyadic Green function method to solve such a problem, we must clarify some aspects connected to the numerical strategy.

A finite-domain time-difference (FDTD) simulation model was applied to analyze the near-field properties around the irradiated nanoparticles [18]. This computational technique is commonly recognized to give an adequate picture of the electromagnetic field distribution in the near- and far-fields around structures with arbitrary shapes. The main signal observed in the FDTD simulation is the Poynting vector of the evanescent wave. Since the z component of the Poynting vector is also the collected signal by the SNOM, the FDTD simulation gives a results that can be immediately compared with the experimental results. However, the observed intensity collected by the SNOM aperture tip needs a comment. As I_{inc}, we choose the incident intensity, averaged over the cross-sectional area of the SNOM aperture tip perpendicular to the Poynting vector ($\boldsymbol{S} = \boldsymbol{E} \times \boldsymbol{H}$) of the evanescent wave, that is spatially characterized by a penetration depth d_p corresponding to the z height of the collecting volume available to the SNOM aperture. Therefore, due to rapid decay of electric fields in the z direction, one additional useful parameter to describe the optical profiles as measured by the SNOM could be the z dependence of the near-field intensity $\mathrm{d}I/\mathrm{d}z$. In our FDTD results, we will calculate this quantity.

In turn, the near-field approximation needs an additional consideration. In the far-field approximation, to exhibit the relative absorption and scattering ability of the NSs, the cross sections for absorption and scattering can be defined as $\sigma_{\mathrm{abs}} = W_{\mathrm{abs}}/I_{\mathrm{inc}}$ and $\sigma_{\mathrm{scat}} = W_{\mathrm{scat}}/I_{\mathrm{inc}}$, respectively, while the efficiencies are defined as $Q_{\mathrm{abs}} = \sigma_{\mathrm{abs}}/A$ and $Q_{\mathrm{scat}} = \sigma_{\mathrm{scat}}/A$ for the absorption and the scattering processes, respectively. Here, if the I_{inc} represents the intensity of the incident wave, $A = \pi r^2$ is the particle cross section projected onto a plane perpendicular to the incident wave, and r is the total radius on the nanosphere.

Finally, the absorption and scattering energy $W_{\mathrm{abs/scat}}$ can be calculated using the Poynting vector integrated over a solid angle [19]; on the other hand, in the near-field, if we consider a

finite dimension of tip aperture, we have that the scattered and absorbed intensities are proportional to the solid angle [20–23].

Therefore, the near-field solution of electric and magnetic fields and the field enhancement in the z direction in the proximity of the SNOM probe tip, under some specific conditions, can provide intense locally enhanced absorption. Since the E_z components under the SNOM tip are about 10 times larger compared to the in-plane components [24–26], it is reasonable to suppose that when the probe signal displays point-like absorption peaks, this can be identified with a nanoshell [10]. This is because the field enhancement caused by the local surface plasmon resonance mainly focuses on the metal–dielectric interface (and decays exponentially) and is not absorbed by the biological tissue due to the NIR transparency window.

3. z-LOCATION PROBLEM OF NPS INSIDE A CELL: THE NEAR-FIELD APPROACH

The z localization of a NS inside the cell requires a near-field approach to calculate the scattering cross section. In particular, we have to consider that the *observer* is the SNOM aperture that we consider as a circular ring located a few nanometers over the cells being scanned. We refer to this question as the *z-location problem*. In the scattering analysis, we have to assume that the NS embedded within the film is small compared to the wavelength. This condition is satisfied because our NSs fall in 100–150 nm diameter range, while the wavelength used is 780 nm. Under this condition, it is widely known that the NS scatters light like an electric point dipole radiates. It is well known that the scattered electric field from the particle can be calculated using Green's dyadic function as

$$\boldsymbol{E}_s(\boldsymbol{r}) = \frac{k_0^2}{\epsilon_0}\boldsymbol{G}(\boldsymbol{r},\boldsymbol{r}_0)\cdot\boldsymbol{p}_0, \tag{1}$$

where $\boldsymbol{E}_s$ is the electric field scattered at the position r in the presence of a point-like dipolar source $\boldsymbol{p}_0$ located at r_0, ϵ_0 is the free-space permittivity, k_0 is the free wavenumber, and $\boldsymbol{G}(\boldsymbol{r},\boldsymbol{r}_0)$ is Green's tensor associated with the whole system. We are assuming that the nanoshell and the background are nonmagnetic ($\mu = 1$), with a relative permittivity ϵ and ϵ_B, respectively. The dyadic Green's function is defined by

$$\nabla\times\nabla\times\boldsymbol{G}(\boldsymbol{r},\boldsymbol{r}') - k_0^2\epsilon(\boldsymbol{r})\boldsymbol{G}(\boldsymbol{r},\boldsymbol{r}') = \delta(\boldsymbol{r}-\boldsymbol{r}'). \tag{2}$$

Thus, if the induced dipole moment is known, the scattered electric field $\boldsymbol{E}_s$ can be easily obtained via the dyadic Green's function. The coordinate system is cylindrical and characterized by choosing the center of the scattering NS particle as $\boldsymbol{r}' = \boldsymbol{r}_0 = z_0\,\hat{z}$.

The local density of plasmonic modes generated by the nanoparticles can be quantified by

$$\rho(\boldsymbol{r},\omega) = \frac{1}{\pi\omega^2 k_0^2\epsilon_0}\,\mathrm{Im}[G(\boldsymbol{r},\boldsymbol{r}')]. \tag{3}$$

In terms of Green's dyadic function, the scattered field $\boldsymbol{E}$ can be obtained by the incident field $\boldsymbol{E}_0$ via the 3D expression,

$$\boldsymbol{E}(\boldsymbol{r}) = \boldsymbol{E}_0(\boldsymbol{r}) + k_0^2\iiint \boldsymbol{G}(\boldsymbol{r},\boldsymbol{r}')\cdot\Delta\epsilon\boldsymbol{E}_0(\boldsymbol{r}')\mathrm{d}\boldsymbol{r}', \tag{4}$$

where $\Delta\epsilon = \epsilon(\boldsymbol{r}) - \epsilon_B$, and ϵ_B is the dielectric constant of the substrate. Equation (4) can be used to compute the Green's function by solving the self-consistent Dyson's equation [27]

$$\boldsymbol{G}(\boldsymbol{r},\boldsymbol{r}') = \boldsymbol{G}_0(\boldsymbol{r},\boldsymbol{r}') + k_0^2\iiint \boldsymbol{G}_0(\boldsymbol{r},\boldsymbol{r}'')\cdot\Delta\epsilon\cdot\boldsymbol{G}_0(\boldsymbol{r}'',\boldsymbol{r}')\mathrm{d}\boldsymbol{r}''. \tag{5}$$

To calculate the scattered part of the electric field in the upper part or substrate, we used the dyadic Green's functions $\boldsymbol{G}>(\boldsymbol{r},\boldsymbol{r}')$ and $\boldsymbol{G}<(\boldsymbol{r},\boldsymbol{r}')$ for $\boldsymbol{r}>z_0$ and $\boldsymbol{r}<z_0$, respectively. In the next sections, we present the near-field dyadic Green's functions following the calculations derived by Jung *et al.* [28]. Following Jung *et al.* [28], the dyadic Green's function $\boldsymbol{G}>(\boldsymbol{r},\boldsymbol{r}')$ and $\boldsymbol{G}<(\boldsymbol{r},\boldsymbol{r}')$ may be expressed in cylindrical coordinate (ρ,φ,z) as

$$\boldsymbol{G}_i^{(s)}(\boldsymbol{r},\boldsymbol{r}_0) = \frac{-i}{4\pi}\int_0^\infty \mathrm{d}\kappa_\rho\frac{e^{\pm i\kappa_{z_i}z}}{\kappa_{z_i}}\xi_{+,i}^{(s)}(\kappa_\rho,z_0,d) \times\left[\frac{J_0'(\kappa_\rho\rho)}{\rho}\hat{\rho}\,\hat{\rho}+\kappa_\rho J_0''(\kappa_\rho\rho)\hat{\varphi}\,\hat{\varphi}\right], \tag{6.a}$$

$$\begin{aligned}\boldsymbol{G}_i^{(p)}(\boldsymbol{r},\boldsymbol{r}_0) = {}& \frac{i}{4\pi k_i^2}\int_0^\infty \mathrm{d}\kappa_\rho\frac{e^{\pm i\kappa_{z_i}z}}{\kappa_{z_i}} \times\left\{\xi_{+,i}^{(p)}(\kappa_\rho,z_0,d)\left[\frac{\kappa_\rho^3 J_0'(\kappa_\rho\rho)}{\kappa_{z_i}}\hat{z}\,\hat{z}\right.\right.\\ & \left.\pm i\frac{\kappa_\rho^2\kappa_{z_r}J_0''(\kappa_\rho\rho)}{\kappa_{z_1}}\hat{\rho}\,\hat{z}\right]\\ & +\xi_{-,i}^{(p)}(\kappa_\rho,z_0,d)\left[-\kappa_{z_i}\kappa_\rho J_0''(\kappa_\rho\rho)\hat{\rho}\,\hat{\rho}\right.\\ & \left.\left.-\kappa_{z_i}\frac{J_0'(\kappa_\rho\rho)}{\rho}\hat{\varphi}\,\hat{\varphi}\;\pm i\kappa_\rho^2 J_0'(\kappa_\rho\rho)\hat{\rho}\,\hat{z}\right]\right\},\end{aligned} \tag{6.b}$$

where J_n is the nth-order Bessel function of the first kind, and the primes on the Bessel functions imply derivatives with respect to the argument. d is the distance between the NS and the SNOM probe aperture, $\kappa_{z_1} = \sqrt{k_i^2 - \kappa_\rho^2}$. The factors $\xi_{\pm,i}^{(x)}(\kappa_\rho,z_0,d)$ are expressed as

$$\xi_{\pm,>}^{(x)}(\kappa_\rho,z_0,d) = \frac{t_>^{(x)}[e^{i\kappa_z(d-z_0)} \pm r_<^{(x)}e^{i\kappa_z(d+z_0)}]}{1 - r_>^{(x)}r_<^{(x)}e^{2i\kappa_z d}}e^{-i\kappa_{z^>}d}, \tag{7.a}$$

$$\xi_{\pm,<}^{(x)}(\kappa_\rho,z_0,d) = \frac{t_<^{(x)}[e^{i\kappa_z z_0} \pm r_>^{(x)}e^{i\kappa_z(2d-z_0)}]}{1 - r_>^{(x)}r_<^{(x)}e^{2i\kappa_z d}}, \tag{7.b}$$

where $r^{(x)}$ denotes the Fresnel reflection coefficients for s and p polarization given by, respectively,

$$r_{>_<}^{(s)} = \frac{\kappa_z - \kappa_{z_{>_<}}}{\kappa_z + \kappa_{z_{>_<}}}, \qquad r_{>_<}^{(p)} = \frac{\epsilon_{>_<}\kappa_z - \epsilon_g\kappa_{z_{>_<}}}{\epsilon_{>_<}\kappa_z + \epsilon_g\kappa_{z_{>_<}}}, \tag{8}$$

so that the transmission coefficients become $t_{>_<}^{(x)} = 1 + r_{>_<}^{(x)}$. Near-field absorption properties of a gold NP require some assumptions, as already mentioned. In particular, we assume that the speed of light is approaching infinity. Thus $\kappa_{z_1} = \sqrt{k_i^2 - \kappa_\rho^2} \to i\kappa_\rho$ and $r_{>_<}^{(s)} \to 0$ $r_{>_<}^{(p)} \to \alpha_{>_<}$, where α is a factor

connected to the plasmon resonance [29]. Using these approximations, we have the following the near-field dyadic Green's function [28]:

$$\boldsymbol{G}_{>}^{(p)}(\boldsymbol{r},\boldsymbol{r}_0)=\frac{i}{4\pi k_{>}^2}\int_0^{\infty}\mathrm{d}\kappa_\rho\kappa_\rho^2 e^{\kappa_\rho z}\times\left\{\xi_{+,>}^{(p)}(\kappa_\rho,z_0,d)[J_0(\kappa_\rho\rho)\hat{z}\,\hat{z}+J_0'(\kappa_\rho\rho)\hat{\rho}\,\hat{z}]+\xi_{-,>}^{(p)}(\kappa_\rho,z_0,d)\left[J_0''(\kappa_\rho\rho)\hat{\rho}\,\hat{\rho}+\frac{J_0'(\kappa_\rho\rho)}{\kappa_\rho\rho}\hat{\varphi}\,\hat{\varphi}+J_0'(\kappa_\rho\rho)\hat{\rho}\,\hat{z}\right]\right\},\tag{9}$$

with

$$\xi_{\pm,>}^{(p)}(\kappa_\rho,z_0,d)=(1-\alpha_>)\cdot(e^{-\kappa_\rho z_0}\mp\alpha_< e^{-\kappa_\rho(2d-z_0)})\sum_{n=0}^{\infty}(\alpha_>\alpha_<)^n e^{-2\kappa_\rho nd}.\tag{10}$$

The z dependence of the near-field intensity in the substrate can be investigated as [27]

$$I_{z>}=\int_{-\infty}^{d}\mathrm{d}z\int_0^{2\pi}\int_0^{\infty}\rho\mathrm{d}\rho\mathrm{d}\varphi|\boldsymbol{E}_{z>}(\boldsymbol{r})|^2,\tag{11}$$

where $\boldsymbol{E}_{z>}$ is calculated from Eq. (1) using the near-field approximation of the dyadic Green's function. Since the imaginary component of the dielectric function of the cell is negligible, we assume the dipole emitter condition and the total near-field power absorbed in the z direction at the edge of the SNOM probe for an illuminating light is $\lambda=780$ nm [28]

$$I_{\mathrm{abs}}=\frac{\omega I_0 d^4\,\mathrm{Im}\,\epsilon_{\mathrm{cell}}\epsilon_0}{96}\sum_{l,k}^{\infty}(\alpha_>\alpha_<)^{l+k}\times\left\{\frac{1}{[d(l+k)+z_0]^3}+\frac{\alpha_<^2}{[d(l+k+2)-z_0]^3}-\frac{2\alpha_>}{[d(l+k+1)]^3}\right\}.\tag{12}$$

The numerical results of the NS z-location question implied in Eqs. (11) and (12) will be presented and discussed in the next section. It must be evidenced that Eq. (12) takes into account only the contribution of the evanescent wave in the z direction because the Poynting vector, and hence energy flow, is along an orthogonal direction with respect to z.

4. NUMERICAL RESULTS AND DISCUSSION

Here, we provide a numerical demonstration of how the near-field approximations of the dyadic Green's function can be used to quantify the electric field at the edge of the SNOM probe tip when the optical response of a NS particle is dominated by near-field absorption. The absorption characteristics of the gold nanoshell are shown in [10]. The NS is considered as a vertical dipole located at $z=0$, and d is the distance between the NS and the SNOM aperture. The distance d is composed by d_1, which is the thickness layer of the cell, and d_2 that is the distance between the SNOM probe and the cell. We assume that the distance d_2 is known and equal to 10 nm, commonly considered as a reasonable value of the probe–sample distance in our SNOM. The SNOM aperture cannot be considered

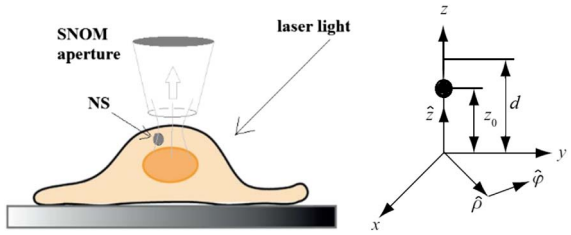

Fig. 2. (Left) Schematic sketch representing the cell + NS sample with the aperture SNOM and (right) the cylindrical systems of coordinates, where d is the potential penetration depth, and z_0 is the localization of the NS with respect to the ground. $d-z_0$ is the distance between the NS and the SNOM probe.

a point since its diameter is approximately 50 nm, while the dimension of the NS is around 120 nm. Such dimensions imply that we have to consider lateral fields in the total sum of the absorbed fields in the z direction. Now, we apply the formalism of Green's method presented in the previous section to obtain the numerical results. The method used is equivalent to the discrete dipole approximation (DDA) method [17]. The system composed of the NS, the cell substrate, and the aperture SNOM, as reported in Fig. 2, is discretized with rectangular parallelepipeds of dimensions $a\times b\times c$. We set parameters a, b, and c as $a=b=c=1$ nm. Using Eq. (12), we calculate the electric field intensity in the z direction for the basin NIR wavelength, which is relevant for our previous experimental results, i.e., $\lambda=780$ nm. The distance between the SNOM aperture and the cell upper edge is set to 10 nm. For sake of simplicity, we consider air ($\epsilon=1$) between the SNOM aperture and the cell. The position of the NS inside the cell is a variable that can change continuously in the range of 10–400 nm and the position of the NS is taken on its upper edge.

One basic contribution of this paper is the accurate determination of the z location of the NS inside the cell. This can be made gaining a deep knowledge of the penetration depth d_p of the collected light from the aperture SNOM. The z decay of a s- or p-polarized electric field is $\sim\exp(-z/d_p)$. The penetration depth expresses the value of z, where the amplitude of the electric field is reduced by a factor $1/e$. The value of d_p is independent of the polarization of the incident light and decreases with the angle of incident light. In our experiment, a fixed angle of incidence of $\theta=45°$ was used for all the measurements. The z component of the electric field is calculated from Eq. (11) and shown in Fig. 3. The resulting penetration depth d_p is ~100 nm. The dipole approximation is considered adequate because, following the DDA approach, only the upper part of the NS is divided into many pieces with similar distances to the SNOM aperture, and then we make a summation. For a small spherical particle, this should correspond to a dipole emitter at a distance of $z_0\sim r$, where r is the NS radius.

Figure 3 shows that the penetration depth available to the aperture SNOM is ~100 nm. To have an immediate representation of this result and its implications for investigations in biology in the NIR transparency windows, we could imagine that the volume inside the cell from which the SNOM probe collected the optical signal is cylinder-like with the base coincident to the SNOM aperture and an height corresponding to

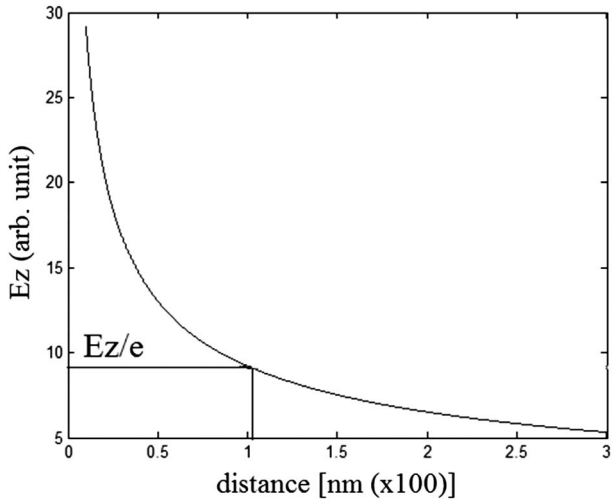

Fig. 3. Calculation of SNOM penetration depth d_p as a function of the SNOM aperture-NS upper part. The SNOM aperture is 50 nm in diameter, the wavelength $\lambda = 780$ nm, and the incidence angle is $\theta = 45°$.

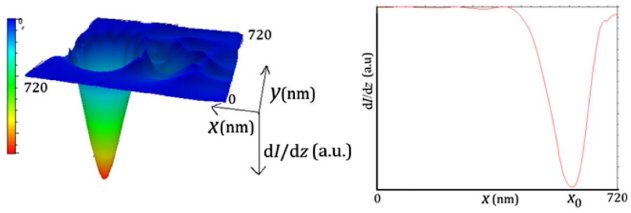

Fig. 4. (Left) Map of signal dI/dz as collected by the aperture SNOM as a function of spatial coordinate xy (720 nm × 720 nm) for a barium titanate-gold NS of 120 nm (80 nm + 40 nm) diameter. The map is made considering the NS located $z = 100$ nm far from the SNOM probe. (Right) Profile of dI/dz as a function of the scanning line x, x_0 denotes the spatial position of the NS. The minimum of dI/dz is reached in correspondence of the NS particle position.

the penetration depth d_p. The map of dI/dz, that is the z derivative of Eq. (12), is shown in Fig. 4 using a FDTD method based on a MATLAB code written *ad hoc* [18].

The intense variation of dI/dz in correspondence of the NS position is in excellent agreement with the experimental results displayed in Fig. 1. This result is particularly meaningful. It demonstrated that inside the penetration depth, the optical signal that corresponds to the total quantity of photons collected by the aperture probe reaches a drastic reduction when the probe is positioned just above the NS.

Figures 3 and 4 represent the original contribution of the present paper. We have demonstrated that when an animal cell is illuminated by NIR light, the transparency window gives the possibility to identify metal nanoparticles when their absorption is particularly intense in the NIR region inside a penetration depth of the cell of approximately 100 nm. Indeed, the cellular membrane, which delimits the boundaries of the cell's body, has a thickness of about 10–15 nm, so any deeper detection below the cell surface must be considered to be intracellular. Our simulation gives confirmation about the experimental results gained using an aperture SNOM. The general analytical and numerical approach used in the present paper can be employed in a wide range of SNOM applications. The extension of our analysis to scattering SNOM is immediate. This result is particularly important for the design of NSs to be applied in hyperthermia cancer treatments [30]. However, other investigations involving near-field plasmonics, biological systems, and scanning optical microscopy can take advantage of our results. In particular, new methods of detection and precise localization of smart nanoparticles, such as these NSs, could promote remarkable spillovers in the emerging field of nanobiomedicine.

5. CONCLUSIONS

Most biological soft tissues have a relatively low light absorption coefficient in the NIR regions—a characteristic known as the tissue optical window. Over such window, near-infrared light transmits through the tissues with scattering-limited attenuation and minimal heating, preventing healthy tissues from being damaged. In this paper, starting from some experimental results previously obtained by our group on the identification of gold NSs inside mouse cells, we numerically demonstrate that an aperture SNOM is able to locate such nanoparticles inside cells with a depth of about 100 nm. This result has been obtained developing a numerical task based on the calculation of the dyadic Green function in the near-field approximation. This result is particularly significant because it gives accurate information about the depth distance for the analysis of the optical properties inside cells under the near-infrared transparency window. This feature is due to a combination of two properties: the NIR transparency of biological systems and the strong absorption capability of appropriate size gold nanoshells in the near-infrared range. Our results can stimulate further developments in the field of thermal treatments of cancers or near-field plasmonic investigations of biological systems.

Acknowledgment. We thank the contribution of the COST Action MP1302 Nanospectroscopy.

REFERENCES

1. S. A. Maier, *Plasmonics: Fundamentals and Applications* (Springer, 2007).
2. K. L. Kelly, E. Coronado, L. L. Zhao, and G. C. Schatz, "The optical properties of metal nanoparticles: the influence of size, shape and dielectric environment," J. Phys. Chem. B **107**, 668–677 (2003).
3. V. Myroshnychenko, J. Rodríguez-Fernández, I. Pastoriza-Santos, A. M. Funston, C. Novo, P. Mulvaney, L. M. Liz-Marzan, and F. J. García de Abajo, "Modelling the optical response of gold nanoparticles," Chem. Soc. Rev. **37**, 1792–1805 (2008).
4. J. B. Jackson, S. L. Westcott, L. R. Hirsch, J. L. West, and N. J. Halas, "Controlling the surface enhanced Raman effect via the nanoshell geometry," Appl. Phys. Lett. **82**, 257–259 (2003).
5. W. E. Doering, M. E. Piotti, M. J. Natan, and R. G. Freeman, "SERS as a foundation for nanoscale, optically detected biological labels," Adv. Mater. **19**, 3100–3108 (2007).
6. A. Cricenti, "Scanning near-field optical microscopy (SNOM)," Phys. Status Solidi C **5**, 2615–2620 (2008).

7. L. R. Hirsch, A. M. Gobin, A. R. Lowery, F. Tam, R. A. Drezek, N. J. Halas, and J. L. West, "Metal nanoshells," Ann. Biomed. Eng. **34**, 15–22 (2006).
8. W. Chen, C. Ayala-Orozco, N. C. Biswal, C. Perez-Torres, M. Bartels, R. Bardhan, G. Stinnet, X.-D. Liu, B. Ji, A. Deorukhkar, L. V. Brown, S. Guha, R. G. Pautler, S. Krishnan, N. J. Halas, and A. Joshi, "Targeting of pancreatic cancer with magneto-fluorescent theranostic gold nanoshells," Nanomedicine **9**, 1209–1222 (2014).
9. C. Liu, C. C. Mi, and B. Q. Li, "Energy absorption of gold nanoshells in hyperthermia therapy," IEEE Trans. Nanobiosci. **7**, 206–214 (2008).
10. M. D'Acunto, A. Cricenti, S. Dinarelli, and M. Luce, "Optical detection of core-gold nanoshells inside biosystems," Nanospectroscopy **1**, 97–105 (2015).
11. D. Sarkar and N. J. Halas, "General vector basis function solution of Maxwell's equations," Phys. Rev. E **56**, 1102–1112 (1997).
12. D. Le, "SURE project, spectroscopic characterization of silica-gold nanoshells," http://www.cmmp.ucl.ac.uk/~mdl/cam/Mie/nanoshells.pdf.
13. J. Feng, V. C. Siu, A. Roelke, V. Metha, S. Y. Rhieu, G. T. R. Palmore, and D. Pacifici, "Nanoscale plasmonic interferometers for multispectral, high-throughput biochemical sensing," Nano Lett. **12**, 602–609 (2012).
14. P. Fan, U. K. Chettiar, L. Cao, F. Afshinmanesh, N. Engheta, and M. L. Brongersma, "An invisible metal–semiconductor photodetector," Nat. Photonics **6**, 380–385 (2012).
15. C. Wu, X. Liang, and H. Jiang, "Metal nanoshells as a contrast agent in near-infrared diffuse optical tomography," Opt. Commun. **253**, 214–221 (2005).
16. G. Mie, "Beiträge zur Optik trüber Medien, speziell kolloidaler Metallösungen," Ann. Phys. **330**, 377–445 (1908).
17. M. D'Acunto, D. Moroni, and O. Salvetti, "Nanoscale biomolecular detection limit for gold nanoparticles based on near-infrared response," Adv. Opt. Technol. **2012**, 1–8 (2012).
18. A. Cricenti, M. Luce, D. Moroni, O. Salvetti, and M. D'Acunto, "Ultrasmall clusters of gold nanoshells detected by SNOM," Optoelectron. Rev. **23**, 39–45 (2015).
19. M. D'Acunto, A. Cricenti, M. Luce, and S. Dinarelli, "Theory of near-field detection of core-gold nanoshells inside biosystems," Comput. Modell. New Technol. **19**, 29–34 (2015).
20. R. Wannemacher, M. Quinten, and A. Pack, "Evanescent-wave scattering in near-field optical microscopy," J. Microsc. **194**, 260–264 (1999).
21. M. Quinten, A. Pack, and R. Wannemacher, "Scattering and extinction of evanescent waves by small particles," Appl. Phys. B **68**, 87–92 (1999).
22. M. Quinten, "Evanescent wave scattering by aggregates of clusters-application to optical near-field microscopy," Appl. Phys. B **70**, 579–586 (2000).
23. A. Y. Bekshaev, K. Y. Bliokh, and F. Nori, "Mie scattering and optical forces from evanescent fields: a complex-angle approach," Opt. Express **21**, 7082–7095 (2013).
24. A. Cricenti, V. Marocchi, R. Generosi, M. Luce, P. Perfetti, D. Vobornik, G. Margaritondo, D. Talley, P. Thielen, J. S. Sanghera, I. D. Aggarwal, J. K. Miller, N. H. Tolk, and D. W. Piston, "Optical nanospectroscopy study of ion-implanted silicon and biological growth medium," J. Alloys Compd. **362**, 21–25 (2004).
25. F. Keilmann and R. Hilenbrand, "Near-field microscopy by elastic light scattering from a tip," Philos. Trans. R. Soc. A **362**, 787–805 (2004).
26. P. Dvorák, T. Neuman, L. Brínek, T. Šamoril, R. Kalousek, P. Dub, P. Varga, and T. Šikola, "Control and near-field detection of surface plasmons interference patterns," Nano Lett. **13**, 2558–2563 (2013).
27. Y. Ould Agha, O. Demichel, C. Girard, A. Bouelier, and G. Colas des Francs, "Near-field properties of plasmonics nanostructures with high aspect ratio," arXiv: 1509.07103v1 2015.
28. J. Jung, T. Søndergaard, T. G. Pedersen, K. Pedersen, A. Nylandsted Larsen, and B. B. Nielsen, "Dyadic Green's functions of thin films: applications within plasmonics solar cells," Phys. Rev. B **83**, 085419 (2011).
29. J. Jung, T. G. Pedersen, T. Søndergaard, K. Pedersen, A. N. Larsen, and B. B. Nielsen, "Electrostatic plasmon resonances of metal nanospheres in layered geometries," Phys. Rev. B **81**, 125413 (2010).
30. D. Sikdar, I. D. Rukhlenko, W. Cheng, and M. Premaratne, "Effect of number density on optimal design of gold nanoshells for plasmonic photothermal therapy," Biomed. Opt. Express **4**, 15–31 (2013).